Matrix-Formation Dynamics Dictate Methyl Nitrite Conformer Abundance

Emily K. Hockey[1], Nathan McLane[2], Korina Vlahos[1], Laura M. McCaslin[3*], Leah G. Dodson[1]*

[1]Department of Chemistry and Biochemistry, University of Maryland, College Park, Maryland 20742, USA
[2]Institute for Physical Science and Technology, University of Maryland, College Park, Maryland 20742, USA
[3]Combustion Research Facility, Sandia National Laboratories, Livermore, California, 94550

Abstract:

Methyl nitrite has two stable conformational isomers resulting from rotation about the primary C-O-N-O dihedral angle: *cis*-CH_3ONO and *trans*-CH_3ONO, with *cis* being more stable by ~5 kJ/mol. The barrier to rotational interconversion (~45 kJ/mol) is too large for isomerization to occur under ambient conditions. This paper presents evidence of a change in conformer abundance when dilute CH_3ONO is deposited onto a cold substrate; the relative population of the freshly deposited *cis* conformer is seen to increase compared to its gas-phase abundance, measured by *in-situ* infrared spectroscopy. We observe abundance changes depending on the identity of the bath gas (N_2, Ar, and Xe) and deposition angle. The observations indicate that the surface properties of the growing matrix influence conformer abundance—contrary to the widely held assumption that conformer abundance in matrices reflects gas-phase abundance. We posit that differences in the angle-dependent host-gas deposition dynamics affect surface morphology, causing changes in conformer abundances. Quantum chemistry calculations of the binding energies between CH_3ONO and a single bath-gas component reveal that the N_2:*cis*-CH_3ONO complex is stabilized relative to the N_2:*trans*-CH_3ONO complex. However, significant energetic stabilization is not observed in 1:1 complexes of Ar:CH_3ONO or Xe:CH_3ONO. From our results, we conclude that the surface morphologies play a significant role in trapping *cis*-CH_3ONO more effectively than *trans*-CH_3ONO, likely because *cis*-CH_3ONO is more compact. Taken together, the observations highlight the necessity for careful characterization of conformers in matrix-isolated systems, emphasizing a need for further study into the deposition dynamics and surface structure of chemically inert matrices.

https://doi.org/10.26434/chemrxiv-2023-4vtc9 **ORCID:** https://orcid.org/0000-0001-5960-056X Content not peer-reviewed by ChemRxiv. **License:** CC BY 4.0

1. Introduction:

Methyl nitrite (CH_3ONO) has received significant experimental[1–32] and theoretical[33–39] investigation focused on its existence as two stable conformational isomers resulting from rotation about the primary C-O-N-O dihedral angle. In ambient conditions, both CH_3ONO *cis* and *trans* rotational isomers can be spectroscopically observed and distinguished from one another using a variety of techniques—gas- and liquid- ^1H NMR, UV-Vis absorption, as well as rotational and vibrational spectroscopy—making conformer-specific studies possible.[3,17,20,23,27]

The barrier to *cis*/*trans* interconversion in the gas phase is relatively high at ~45 kJ/mol due to contribution of resonance structures with planar C-O-N-O atoms.[5,33] The relative energies of the two stable conformers differ by ~5 kJ/mol, with *cis*-CH_3ONO being the more stable of the two.[1,3,17,20,23] Other RONO molecules can exhibit steric repulsions that result in larger differences between conformer energies and thus abundances.[11–13,24] In the case of CH_3ONO, the *cis*-CH_3ONO conformer is stabilized via internal hydrogen bonding, orienting the N=O portion of the C-O-N-O dihedral towards the methyl group, resulting in a smaller van der Waals diameter than *trans*-CH_3ONO.[3,17,20,23,24,34,36]

The determination of conformer abundance of CH_3ONO becomes increasingly complicated when moving away from the gas-phase into complex environments such as those found in matrix-isolation spectroscopy. In general, matrix-isolation experiments assume that matrix conformer abundances reflect gas-phase abundances. Upon deposition, this retention of the gas-phase abundance results in matrix abundances that are not in thermal equilibrium at the colder matrix temperature. In some cases the ratio of two or more conformers present in the gas phase can change upon isolation in a low-temperature matrix.[15,40–47] Typically this is only observed for chemical systems with a small (< 5 kJ/mol) barrier to isomerization; as the molecules isomerize, their relative conformer abundances equilibrate to the abundances expected at the lower temperature of the matrix. This is a phenomenon known as conformational cooling.[42,46–48] For molecules with higher interconversion barriers similar to that seen in CH_3ONO, there are typically no significant changes in the conformer abundance between the gas and matrix phases.[15,19,49–51] The complex dynamics of the matrix-formation process and subsequent diffusion of molecules on the surface of a growing matrix are rarely discussed as contributing factors in possible differing conformer abundances between the gas and matrix phases. Theoretical and experimental work focusing on the sticking dynamics, energy transfer, and angle dependence of deposition are typically confined to atoms and molecules sticking to a metal surface or molecular ices, not on inert matrices.[52–75] To the authors' knowledge, the impact of these factors on conformer abundance in inert matrices has not been quantified.

We performed a study on the effects of a given bath gas and the angle of deposition on the conformer abundance of CH_3ONO during deposition in a low-temperature matrix using three different inert bath gases: nitrogen (N_2), argon (Ar), and xenon (Xe). Our observations indicate a change in conformer abundance that occurs between the gas and matrix phases. Changes to deposition angle were additionally found to alter conformer abundances in a N_2 bath gas, while conformer abundances in Ar showed no angular dependence. We investigate the competition between effects of surface morphology and energetic stabilization on the trapping of the two conformers by analyzing the angular dependence of the abundances and performing quantum chemistry calculations of the gas:CH_3ONO complexes. We propose that the surface formation dynamics of N_2 change with the angle of deposition, affecting the conformer abundance. Quantum chemistry calculations of N_2:CH_3ONO also indicate that *cis*-CH_3ONO is energetically stabilized relative to *trans*-CH_3ONO. Quantum chemistry calculations of X:CH_3ONO (X = Ar, Xe) do not

https://doi.org/10.26434/chemrxiv-2023-4vtc9 **ORCID:** https://orcid.org/0000-0001-5960-056X Content not peer-reviewed by ChemRxiv. **License:** CC BY 4.0

indicate significant stabilization of either conformer. We thus attribute the increase in *cis*-CH_3ONO abundance in Ar and Xe matrices to its smaller van der Waals radius, enhancing the probability of trapping within pockets during surface diffusion. These size effects are also likely to contribute to the enhancement of *cis*-CH_3ONO in N_2.

2. Methods

The conformer abundance of CH_3ONO was investigated using matrix-isolation spectroscopy. The next sections describe the methods in detail, which are summarized first: CH_3ONO is diluted in one of three different bath gases—N_2, Ar or Xe—and individual mixtures are deposited at varying angles onto a cold substrate where they form a low-temperature matrix at controlled temperatures. Spectroscopic analysis using a Fourier-Transform infrared (FTIR) spectrometer is employed. Conformer-specific vibrational bands in the infrared spectrum are integrated and compared to quantify the conformer abundance of *cis*-CH_3ONO compared to *trans*-CH_3ONO. These conformer abundances are compared with gas-phase measurements to determine the degree of change. Quantum chemistry calculations are performed to quantify binding energies between matrix-gas molecules and the two conformers of CH_3ONO.

2.1. Experimental

The matrix-isolation spectrometer has been described in detail previously.[76] Briefly, the matrix-isolated sample is prepared in the center of the chamber on a 1-inch KBr salt-glass substrate that is cooled by a CTI Model 22 cryocooler. The temperature of the sample holder is monitored and controlled through both a silicon diode and resistive heaters connected to a Lakeshore Model 331 temperature controller. A differentially pumped rotary platform enables the sample to rotate 360° inside the chamber without breaking the vacuum. In practice, the sample mount either faces towards the deposition axis where sample/matrix gases are deposited or is rotated into alignment with the optical axis for spectroscopic analysis. The chamber maintains a base pressure of ~8×10^{-8} Torr, and reaches ~8×10^{-9} Torr with cryopumping.

CH_3ONO is synthesized in house using air-sensitive techniques according to previous literature,[3] with no further purification necessary. Briefly, sodium nitrite (ACS grade, 97%) is dissolved in a solution of water and methanol (HPLC grade, >99.8%) and allowed to stir at room temperature under an inert atmosphere. Then, hydrochloric acid (ACS grade, 36.5-38%) is titrated into the aqueous solution. The gaseous CH_3ONO that evolves from the solution is passed through a drying tube before being collected in a liquid nitrogen trap. After the condensed CH_3ONO sublimates at room temperature, it is immediately diluted to concentrations less than 10% in N_2 (Airgas, Industrial Grade), Ar (Airgas, UHP), or Xe (Spectra Gases, UHP) in a stainless-steel cylinder. CH_3ONO is known as a highly flammable, heat-sensitive explosive. Therefore, we ensure each cylinder is diluted to concentrations of 10% or less in order to minimize the hazards of working with CH_3ONO in a confined laboratory space.

From these dilute cylinders, 500:1 mixtures of X:CH_3ONO (where X= N_2, Ar, Xe) are prepared manometrically. The room-temperature gaseous mixtures are deposited onto the cold substrate in the matrix-isolation chamber through an effusive source immediately forming amorphous matrices. The substrate is held at 10 K during deposition for mixtures containing N_2 and Ar, and 30 K for mixtures containing Xe. Deposition rates are controlled by a dosing valve (VAT), and deposition times range from 1.5–6 hours. The angle of deposition, defined from the plane perpendicular to the cold substrate (denoted as α), varied from −10° to 20°. For reference, a gas

https://doi.org/10.26434/chemrxiv-2023-4vtc9 **ORCID:** https://orcid.org/0000-0001-5960-056X Content not peer-reviewed by ChemRxiv. **License:** CC BY 4.0

deposited normal to the cold substrate would have an α angle of 0°, and any other angle would be considered an oblique angle deposition (OAD). The range of angles is restricted by the design of the aluminum heat shield attached to the first stage of the cryostat, thus limiting the range of deposition angles possible.

The infrared (IR) spectrum of the matrix-isolated sample is collected from a single pass of the externally coupled FTIR beam through the matrix-isolation chamber and sample before being focused into the external MCT-A detector. The FTIR is equipped with a broadband KBr beamsplitter, limiting the spectral range to 7400–600 cm^{-1}. The spectra are recorded with a resolution of 0.5 cm^{-1}—which corresponds to a data spacing of 0.241 cm^{-1}—and background subtracted. Spectroscopic signatures corresponding to each conformer are integrated using OriginPro to determine the *cis* and *trans* conformer total absorbances.

For gas-phase experiments, the IR spectrum is obtained using the same FTIR. Instead of externally coupling the IR beam to the matrix-isolation chamber, the IR beam remains internal, making a single pass through a gas cell that is located in the main sample compartment of the FTIR, before being focused into a deuterated triglycine sulfate (DTGS) detector. The threaded gas cell with J. Young® Valve (Thorlabs) is equipped with two MgF_2 windows, limiting the low-frequency spectral range. The spectra are recorded with a resolution of 0.125 cm^{-1}—which corresponds to a data spacing of 0.015 cm^{-1}—and background subtracted. The *cis*- and *trans*-ν_3 modes of the gas-phase CH_3ONO spectra are fit using the Multipeak Fitting package in IgorPro, defined by a Gaussian line profile (see Supplementary Material (SM), Section 2). The area of these fits is used to determine the integrated absorbance of each transition in the gas phase.

The percentage of each conformer is calculated by dividing the concentration of a given conformer (*cis* or *trans*) by the sum of the concentrations of both conformers (*cis* and *trans*) for a specific vibrational transition, which can also be expressed in terms of integrated absorbance through Beer's Law:

$$\%\, trans = \frac{c_{trans}}{c_{cis} + c_{trans}} \times 100 = \frac{\frac{A_{trans}}{A_{cis}}}{\frac{A_{trans}}{A_{cis}} + 1} \times 100$$

This treatment assumes that the absorption coefficient for comparable vibrational modes (e.g. the ν_3 N=O stretch) is the same in each conformer (see SM, Section 1 for detailed explanation). This assumption leads to a relative error in the calculated abundance percentages on the order of 4% in matrix-phase samples for the ν_3 vibrational mode of CH_3ONO.

2.2. Computational

All quantum chemical computations were performed with Q-Chem 5.4.[77] Minimum energy structures of both *cis* and *trans* conformers of CH_3ONO bound to a single matrix-gas component, X:CH_3ONO (X = N_2, Ar, or Xe), are calculated. Twenty-two initial configurations of each 1:1 complex were generated, with the bath gas placed around either the *cis*-CH_3ONO or *trans*-CH_3ONO molecule. Geometry optimizations were performed using the B3LYP density functional[78,79] with Grimme's D3(BJ) dispersion correction[80] and cc-pVDZ basis set.[81,82] For Xe, the cc-pVDZ-PP basis set and corresponding ECP were used.[83] Zero-point energy corrections were computed via harmonic frequency analysis at the same level of theory. Relative energies of the clusters are refined via single-point energy calculations with coupled cluster theory, employing single, double and perturbative triple excitations, CCSD(T)[84,85], and an aug-cc-pVDZ basis set[81,82] for all atoms except Xe, for which the aug-cc-pVDZ-PP basis and corresponding ECP were used.[83]

https://doi.org/10.26434/chemrxiv-2023-4vtc9 **ORCID:** https://orcid.org/0000-0001-5960-056X Content not peer-reviewed by ChemRxiv. **License:** CC BY 4.0

Binding energies of the X:CH_3ONO complex were computed as differences in the zero-point energy corrected CCSD(T) single-point energies between the X:CH_3ONO complex and infinitely separated X compound and CH_3ONO molecule.

3. Results

The aim of this work is to investigate the competition between energetic stabilization and surface morphological effects that lead to changes in CH_3ONO conformer abundance ratios between the gas phase and different low-temperature matrices. Gaseous CH_3ONO was analyzed to confirm the room-temperature *cis* and *trans* conformer abundances in the bath gases before deposition into the matrix chamber. Upon condensation of the room-temperature CH_3ONO in three different matrices— N_2, Ar, Xe —the *cis* and *trans* conformer abundances are seen to change in varying amounts, but always favoring an increase in the proportion of the *cis* conformer. Furthermore, when the angle of deposition is changed, we see additional changes in the conformer abundances. Quantum chemistry calculations of the 1:1 complexes help to uncover the effects of relative energetic stabilization and relative size of the conformers.

3.1. Gas-Phase Conformer Abundance

Dilute gaseous standards of CH_3ONO in N_2 and Ar were used to calculate conformer abundance in the gas phase using FTIR spectroscopy. The standards were composed of varying concentrations of X:CH_3ONO, where X = N_2 or Ar. Xe was excluded from the gas-phase experiments due to the worldwide shortage in the gas supply. IR transition frequencies corresponding to each isomer were identified based on previous literature, with *cis* centered at 1623 cm^{-1} and *trans* observed at 1680 cm^{-1}.[7,17,18,26] The abundance of each conformer in the gas phase was quantified by comparing the integrated areas under the peaks corresponding to the fundamental N=O stretch ν_3 (see Supplemental Material (SM), Section 2). The average room-temperature *cis* and *trans* conformer relative abundances were determined to be 57 ± 2% to 43 ± 2%, respectively, regardless of bath gas. Previous studies have shown that the ν_3 stretch of *cis* and *trans*-CH_3ONO have approximately the same absorption cross section[23,25] and we use this assumption here, with further details given in SM, Section S1, to equate absorbance ratios with concentration ratios. Our experimentally determined *cis* and *trans* gas-phase abundances are in good agreement with previous observations that used gas-phase IR spectroscopy to determine conformer abundances at room temperature.[3,26]

3.2. Freshly Deposited Matrix-Isolated Conformer Abundance

To investigate changes in the conformer abundance between gas phase and different low-temperature matrices, dilute samples of CH_3ONO in different bath gases were condensed onto a cold substrate at an angle of $\alpha = 20°$, and conformer abundances in the matrix were measured using matrix-isolation spectroscopy (see **Fig. 1**). Due to the inherent narrow line width of matrix-isolated vibrational transitions, the *cis* and *trans* conformer transitions of CH_3ONO are distinguishable,[4,10,14–16,26,86] regardless of the spectral region.

Fig. 1 compares the freshly deposited—as opposed to matrices that have undergone annealing or other processing—matrix-isolated spectra of the fundamental N=O stretch ν_3 of 500:1 X:CH_3ONO, (X = N_2, Ar, Xe) from 1690–1590 cm^{-1} deposited at $\alpha = 20°$. Full matrix-isolated spectra from 3500–700 cm^{-1} for each matrix at this angle can be found in SM Section 3. The most

https://doi.org/10.26434/chemrxiv-2023-4vtc9 **ORCID:** https://orcid.org/0000-0001-5960-056X Content not peer-reviewed by ChemRxiv. **License:** CC BY 4.0

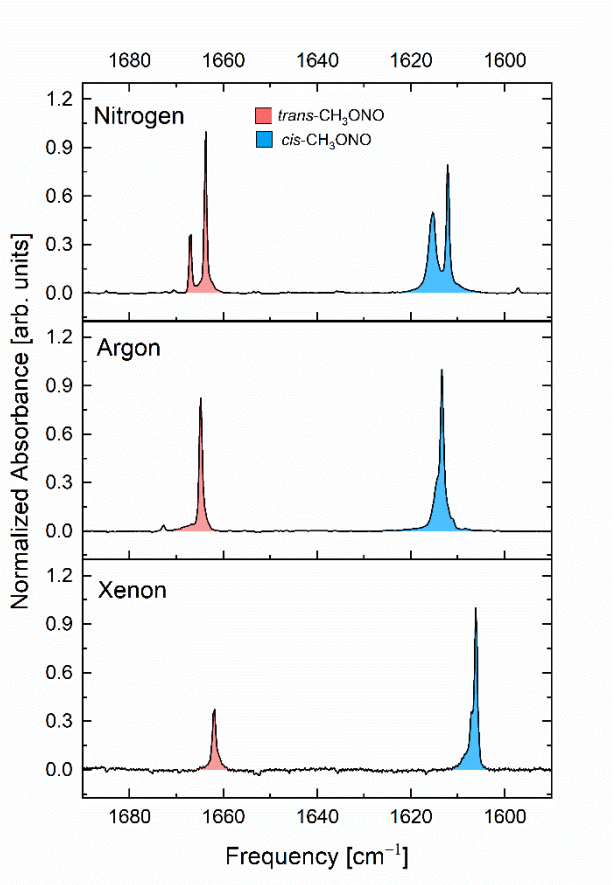

Fig. 1. Normalized matrix-isolated infrared spectra of the region corresponding to the ν_3 transition of CH_3ONO (1690–1590 cm^{-1}), shown for different low-temperature matrices. The deposition angle was fixed at $\alpha = 20°$ and the pre-mixed concentration remained constant at 500:1 X:CH_3ONO, where X = N_2 (top), Ar (middle), or Xe (bottom). The spectra have been color-coded showing regions assigned to the *cis* (blue) and *trans* (pink) conformers.

intense transition in this spectral region (whether it corresponds to *cis*-ν_3 or *trans*-ν_3 CH_3ONO) was normalized to 1, and the absorbance of the remainder of the spectrum was scaled linearly. The *cis*-ν_3 transition in N_2 is centered at 1612 cm^{-1} with a secondary peak centered at 1615 cm^{-1} (more details on secondary peaks in the next paragraph), in Ar is centered at 1613 cm^{-1}, and in Xe is centered at 1606 cm^{-1}. The *trans*-ν_3 transition in N_2 is centered at 1664 cm^{-1} with a secondary peak centered at 1667 cm^{-1}, in Ar is centered at 1665 cm^{-1}, and in Xe is centered at 1662 cm^{-1}.

We observe differences between the spectra of matrix-isolated CH_3ONO and the gas-phase spectra of CH_3ONO (See SM, Section 2) that are all typical of matrix-isolation spectroscopy, in addition to the observed differences between the spectra obtained with different matrix hosts; the latter being the focus of this work. First, a single transition of CH_3ONO (in this case, the *cis*-ν_3 or the *trans*-ν_3) has its vibrational energy shifted compared to that of the unperturbed gas-phase transition—otherwise known as a "matrix shift." These matrix shifts can depend on: (a) the degree of weak interaction between the matrix material and the guest molecule, and (b) the specific vibrational mode of the trapped molecule.[40,41] Different vibrational modes can be perturbed to different degrees due to the orientation of the trapped molecule inside the matrix cage, thus introducing a larger (or smaller) matrix shift. However, conformer assignment of the matrix-

https://doi.org/10.26434/chemrxiv-2023-4vtc9 **ORCID:** https://orcid.org/0000-0001-5960-056X Content not peer-reviewed by ChemRxiv. **License:** CC BY 4.0

isolated spectrum of CH_3ONO is unambiguous and the matrix shift has no effect on measured abundances. Secondly, the total intensity of a given transition can be split into multiple peaks (as seen most clearly in the top N_2 trace of **Fig. 1**) due to the guest molecule being trapped in differing matrix sites, otherwise known as "site splitting." Typically, site splitting is only observed to create secondary peaks within a few cm^{-1} of the most stable site.[40,41] We integrate over all peaks within a given transition in order to incorporate all configurations of a given conformer. The final difference between gas- and matrix-isolated spectra, as mentioned previously, is the narrow line width of the matrix-isolated transitions. This is in part due to the majority of the rotational energy being quenched in the matrix, allowing the main spectroscopic feature to be a defined single band and enabling straightforward integration in conformer analysis.[40,41]

We integrated the *cis* and *trans*-ν_3 transitions in the N_2 matrix spectrum in the top trace of **Fig. 1**, identifying an increase in the population of the more stable conformer *cis*-CH_3ONO in the matrix relative to that of the gas phase. The *cis* and *trans* conformer abundances of the freshly deposited N_2 matrix are 65 ± 3% to 35 ± 1%, respectively, when deposited at 20°. This increase in the *cis*-CH_3ONO population by ~15% contradicts previous literature showing that CH_3ONO retains its gas-phase conformer abundance;[15,19] our results indicate that the assumption that conformer abundances in matrix-isolation experiments reflect gas phase abundances may not always hold.

We also observe an increase in the *cis* abundance in Ar and Xe matrices when comparing to the gas-phase abundances. When CH_3ONO is isolated in an Ar matrix with a deposition angle of α = 20°, we observe the *cis* and *trans* conformer abundances to be 63 ± 3% to 37 ± 1%, respectively, shown in the middle trace of **Fig. 1**. There is an ~11% increase in the *cis*-CH_3ONO population in the freshly deposited Ar matrix compared to the gas-phase abundances. Lastly, integration of the ν_3 transitions in the Xe matrix, shown at α = 20° in the bottom trace of **Fig. 1**, results in measured *cis* and *trans* abundances of 73 ± 3% to 27 ± 1%, respectively, corresponding to a ~30% increase in the *cis*-CH_3ONO abundance in the Xe matrix compared to its gas-phase abundance. All *cis* and *trans* conformer abundances in each freshly deposited matrix and the gas-phase conformer abundance are summarized in **Table 1.**

Table 1. Matrix-isolated conformer-specific abundances measured using the *cis* and *trans*-ν_3 transition of freshly deposited X:CH_3ONO (where X = N_2, Ar, Xe) at α = 20° compared to the room temperature (RT) dilute gas-phase conformer abundance.

Composition of Host Matrix (deposition temperature in parentheses)	*cis*-CH_3ONO	*trans*-CH_3ONO
None (RT Gas Phase)	57 ± 2%	43 ± 2%
Nitrogen (10 K)	65 ± 3%	35 ± 1%
Argon (10 K)	63 ± 3%	37 ± 1%
Xenon (30 K)	73 ± 3%	27 ± 1%

A change in conformer abundance in freshly deposited matrix-isolated CH_3ONO was unexpected, regardless of the matrix host, since this phenomenon is typically only observed in cases where the internal conversion barrier between conformers is relatively low. When these barriers are small, conformer interconversion can occur, allowing abundances to approach thermodynamic equilibrium at the lower temperature of the matrix; this is known as conformational cooling. However, the interconversion barrier between *trans* and *cis*-CH_3ONO

https://doi.org/10.26434/chemrxiv-2023-4vtc9 **ORCID:** https://orcid.org/0000-0001-5960-056X Content not peer-reviewed by ChemRxiv. **License:** CC BY 4.0

(~45 kJ/mol) is too large for isomerization to occur at any matrix temperature used in this study. We therefore must consider other physical mechanisms responsible for our observed changes in conformer abundance between the gas and matrix phases, as well as the observed lower-energy conformer enrichment following a *cis* abundance enhancement of $N_2 \approx Ar < Xe$.

3.3. Angular Dependance of Conformer Abundance

One parameter that could alter the observed conformer abundances is the deposition angle. To test for such angular dependence, dilute samples of 500:1 CH_3ONO in different bath gases were condensed onto a cold substrate at different deposition angles, ranging from $\alpha = 20°$ and $\alpha = -10°$ in increments of 10°. Due to the symmetry of the experimental setup, negative deposition angles should yield the same results as their corresponding positive angles, though small deviations in results may occur due to changes in the orientation of the heat shield relative to the beam (see Section 2.1 for more details). Conformer abundances in the matrix were measured using matrix-isolation spectroscopy (see SM Section 5, Figure S6) and compared as before to the gas-phase abundance.

After integrating the *cis* and *trans*-ν_3 transition for each angle α, we observe a decrease of the proportion of *cis*-CH_3ONO as α deviates from 0° when using N_2 as the matrix host with a 500:1 N_2:CH_3ONO ratio. When $\alpha = 20°$, the conformer abundance is 65% ± 3% *cis*-CH_3ONO and 35% ± 1% *trans*-CH_3ONO, as shown in Section 3.2. When α is decreased to $\alpha = 10°$, the conformer abundance becomes 61% ± 3% *cis* and 39% ± 1% *trans*-CH_3ONO. Changing the deposition angle by 10 degrees once more to achieve $\alpha = 0°$—a perpendicular deposition—the conformer abundance is observed to be 58% ± 3% *cis* and 42% ± 1% *trans*-CH_3ONO. Interestingly, the conformer abundance observed after a head-on deposition is nearly the room-temperature gas-phase conformer abundance, in agreement with the sudden-trapping assumption typical for matrix-isolation experiments. Passing perpendicular, the deposition angle was altered a final time to $\alpha = -10°$. At this deposition angle we observe the conformer abundance reverts back towards a greater enhancement in *cis*-CH_3ONO, resulting in 63 ± 3% *cis* and 37 ± 1% *trans*-CH_3ONO. These results, as seen in **Fig. 2**, show that when CH_3ONO in N_2 is deposited at a larger angle of deposition, there is an enhancement of *cis*-CH_3ONO.

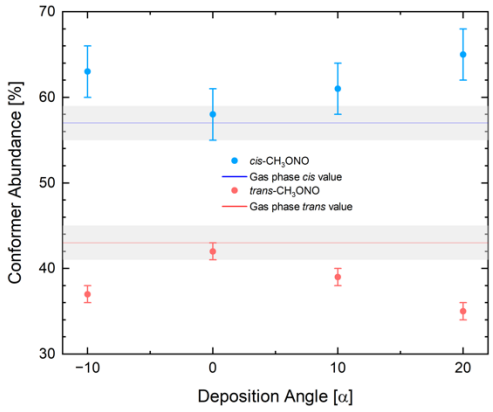

Fig. 2. Conformer abundance of matrix-isolated CH_3ONO in N_2 as a function of deposition angle (α) of the *cis* (blue) and *trans* (pink) ν_3 transition of 500:1 N_2:CH_3ONO observed between 1690–

https://doi.org/10.26434/chemrxiv-2023-4vtc9 **ORCID:** https://orcid.org/0000-0001-5960-056X Content not peer-reviewed by ChemRxiv. **License:** CC BY 4.0

1590 cm^{-1}. The blue and red solid lines represent the gas-phase conformer abundance of 57 ± 2% to 43 ± 2%, where the gas-phase abundance errors are represented in shaded grey.

The angle of deposition for 500:1 Ar:CH_3ONO was altered from $\alpha = -10°$ and $\alpha = 20°$, keeping the remaining experimental conditions constant (see SM Section 5, Figure S7). As stated in Section 3.2, integrating the *cis* and *trans*-ν_3 transition when CH_3ONO was deposited in Ar at α = 20° produced 63% ± 3% *cis*-CH_3ONO and 37% ± 1% *trans*-CH_3ONO. Decreasing the incidence of deposition (towards a more head-on angle) to α = 10°, we observe no statistically significant (outside of the largest reported 1σ error) change of the *cis* and *trans* abundances, with observed *cis* and *trans* abundances of 62% ± 3% to 38% ± 1%, respectively. Once more, the deposition angle was changed by 10 degrees in order to reach α = 0°, where the deposition angle is perpendicular to the cold substrate. In this head-on configuration, we again observe the *cis* conformer abundance to be 62% ± 3% and the *trans* conformer abundance to be 38% ± 1%. Finally, the angle of deposition was altered past perpendicular by 10 degrees, to $\alpha = -10°$. We once again do not observe a statistically significant change in conformer abundance, resulting in 61 ± 3% *cis* and 39 ± 1% *trans*-CH_3ONO. The *cis* and *trans* isomer abundances quantified in an Ar matrix across the angles within this study never approached the ratio observed in the gas phase, as shown in **Fig. *3***. The *cis* and *trans* conformer abundances of N_2 and Ar matrices deposited at different angles are summarized in **Table 2**.

It would be reasonable to expect the results of the Xe matrix to be similar to those of Ar, since both are atomic matrices. However, the even larger enhancement of *cis*-CH_3ONO when deposited onto a Xe surface alludes to more complicated dynamics at play. In matrix-isolation experiments and molecular dynamics (MD) simulations—specifically those that include guest species with more than one conformer—Xe has consistently been an outlier, and explaining the observations of isolated molecules becomes difficult with the possibility of heavy atom perturbation.[46,48,87–93] While we believe that performing OAD experiments with a Xe matrix would provide more information for understanding the conformer abundance when CH_3ONO is isolated in different low-temperature inert matrices, additional angle-dependent experiments in the Xe matrix would not be reasonable to pursue given current Xe availability. We maintain that it is important to show the change between two atomic matrices deposited at the same angle (α = 20°), reinforcing that gas/surface processes are complex even between similar systems.

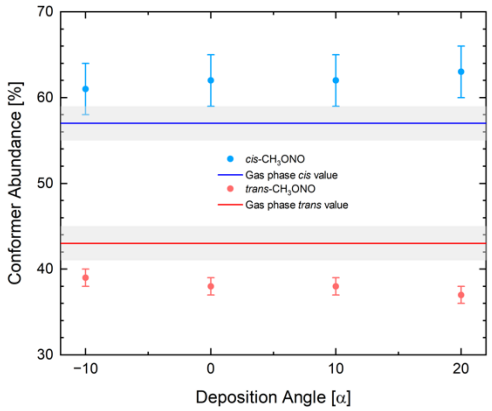

Fig. 3. Conformer abundance of matrix-isolated CH_3ONO in Ar as a function of deposition angle (α) of the *cis* (blue) and *trans* (pink) ν_3 transition of 500:1 Ar:CH_3ONO observed between 1690–

https://doi.org/10.26434/chemrxiv-2023-4vtc9 **ORCID:** https://orcid.org/0000-0001-5960-056X Content not peer-reviewed by ChemRxiv. **License:** CC BY 4.0

1590 cm^{-1}. The blue and red solid lines represent the gas-phase conformer abundance of 57 ± 2% to 43 ± 2%, where the gas-phase abundance uncertainty is represented in shaded grey.

Table 2. Conformer abundance of freshly deposited 500:1 X:CH_3ONO (where X = N_2 or Ar) at different deposition angles.

	Nitrogen		Argon	
Deposition Angle (α)	*cis*-CH_3ONO	*trans*-CH_3ONO	*cis*-CH_3ONO	*trans*-CH_3ONO
−10°	63 ± 3%	37 ± 1%	61 ± 3%	39 ± 1%
0°	58 ± 3%	42 ± 1%	62 ± 3%	38 ± 1%
10°	61 ± 3%	39 ± 1%	62 ± 3%	38 ± 1%
20°	65 ± 3%	35 ± 1%	63 ± 3%	37 ± 1%

The angle-dependent observations further demonstrate changes in conformer abundances that cannot be explained by a conformational cooling mechanism. In light of the differences observed between different bath gases, we consider differences in the dynamics of matrix deposition between the conformers, including structural and energetic effects. We thus turn to quantum chemistry calculations of 1:1 binding complexes to guide our interpretation.

3.4. Calculations of 1:1 X:CH_3ONO Binding Energies

In this section, we compare the intermolecular interactions between CH_3ONO and each matrix gas by calculating the binding energies of simple 1:1 complexes (one CH_3ONO molecule associated with one bath-gas atom or molecule). We use these 1:1 cluster calculations to identify the range of binding energies for different configurations and conformers. While we recognize the limitations of such models for reproducing binding energies between a complex matrix surface and CH_3ONO, calculations of CH_3ONO and model matrix surfaces are not performed due to significant computational expense. Furthermore, relevant surface morphologies, which are dynamical quantities, are unknown, increasing the difficulty of developing an appropriate model. With these caveats in mind, we analyze the high-level quantum chemistry calculations of gas:CH_3ONO clusters. For reference, the energy difference between *cis*-CH_3ONO and *trans*-CH_3ONO—defined as the energy of the *cis* conformer minus the energy of the *trans* conformer in the absence of a bath gas—is −4.39 kJ/mol.

https://doi.org/10.26434/chemrxiv-2023-4vtc9 **ORCID:** https://orcid.org/0000-0001-5960-056X Content not peer-reviewed by ChemRxiv. **License:** CC BY 4.0

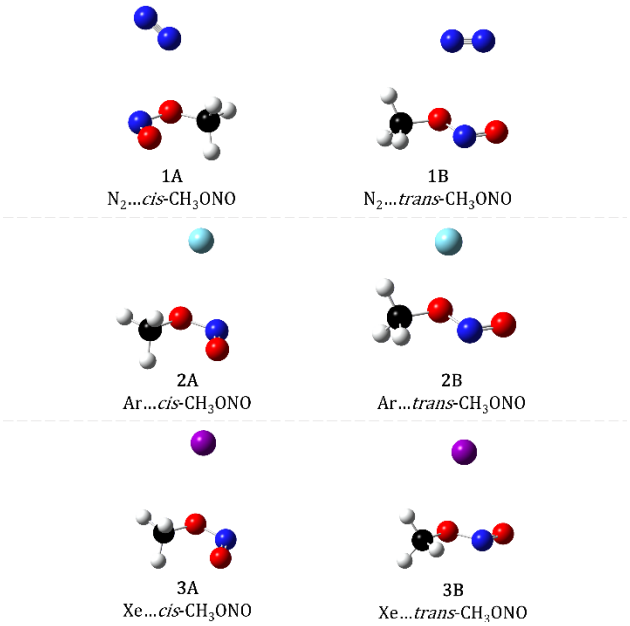

Fig. 4. Structural minima for 1:1 complexes of X…CH_3ONO, where X = N_2 (1A and 1B), Ar (2A and 2B) found at the B3LYP-D3/cc-pVDZ level of theory for structures containing N_2 and Ar. Structural minima for 1:1 complexes of X…CH_3ONO where X = Xe (3A and 3B) found at the B3LYP-D3/cc-pVDZ-PP with corresponding ECP. Carbon (black), nitrogen (blue), oxygen (red), hydrogen (white), argon (teal), and xenon (purple).

We begin our binding energy analysis with the 1:1 complexes formed with N_2. From the 22 structures of each conformer evaluated as part of our survey, we identified the lowest energy 1:1 complexes that contain a single N_2 molecule and a given conformer of a CH_3ONO molecule, shown **Fig. 4**, and calculated the binding energies relative to the separated monomers. The binding energy of minimum-energy structure for the *cis* conformer (1A) is −5.42 kJ/mol, whereas the binding energy of the minimum-energy *trans* structure (1B) is −4.35 kJ/mol, see **Table 3**. The difference in complex binding energies—defined as the 1:1 complex binding energy containing the *cis* conformer minus the 1:1 complex binding energy containing the *trans* conformer ($\Delta E_{cis} - \Delta E_{trans}$) for a common bath gas—suggest a difference of −1.08 kJ/mol. The negative energy difference indicates that the N_2-van der Waals complex containing the *cis* conformer is more stable than that containing the *trans* conformer. For all optimized geometries of N_2:CH_3ONO, the average binding energy of complexes containing the *cis* conformer is −3.97 kJ/mol, while all complexes containing the *trans* conformer have an average binding energy of −3.36 kJ/mol, see **Table 4**. Even when considering all possible orientations that result when CH_3ONO and N_2 form a stabilizing interaction, the difference in average binding energies is −0.61 kJ/mol, where complexes containing *cis*-CH_3ONO demonstrate a slight additional stabilization compared to complexes containing *trans*-CH_3ONO. The preferential binding of N_2 to *cis*-CH_3ONO will be discussed in light of the experimentally observed enhancement in Section 4.

The binding energies of the lowest energy complex containing a single Ar atom and a CH_3ONO molecule are −3.73 kJ/mol for the *cis* conformer (2A), and −3.43 kJ/mol for the *trans* conformer (2B), see **Table 3**. This calculation again suggests that the difference in binding energies is −0.30 kJ/mol, where there is slight preference for the *trans* conformer compared to the *cis* conformer. Considering all optimized geometries of Ar:CH_3ONO, the average binding energy of complexes involving the *cis* conformer is −2.37 kJ/mol and complexes involving the *trans* conformer is −2.79

https://doi.org/10.26434/chemrxiv-2023-4vtc9 **ORCID:** https://orcid.org/0000-0001-5960-056X Content not peer-reviewed by ChemRxiv. **License:** CC BY 4.0

kJ/mol, see **Table 4**. The difference in average binding energies of all stabilizing complexes is +0.12 kJ/mol. The lack of substantial preferential binding of Ar to *trans*-CH_3ONO over *cis*-CH_3ONO will be discussed in comparison with the experimental findings in Section 4.

Finally, for the lowest energy 1:1 complex containing a single Xe atom and a CH_3ONO molecule, the binding energy of the complex containing the *cis* conformer (3A) is −6.11 kJ/mol, while the complex containing the *trans* conformer (3B) binding energy is −6.13 kJ/mol, see **Table *3***. A binding energy difference of +0.03 kJ/mol between the *cis* and *trans* complexes with Xe suggests that there is little preference for conformer. When considering all optimized geometries of Xe:CH_3ONO, the average binding energy for complexes containing a *cis* conformer is −4.99 kJ/mol. The average binding energy between Xe and the trans conformer is −4.76 kJ/mol, see **Table 4**. For all optimized geometries, the calculations suggest that the *cis* and *trans* conformers do not exhibit preferential binding to a particular conformer. These results will be discussed in comparison to the experimental findings in Section 4.

Table 3. Summary of the binding energy of the lowest energy 1:1 complex of X…CH_3ONO, where X = N_2, Ar, or Xe.

	$\Delta \boldsymbol{E}$ of X…*cis*-CH_3ONO (kJ/mol)	$\Delta \boldsymbol{E}$ of X…*trans*-CH_3ONO (kJ/mol)	$\Delta \boldsymbol{E}_{cis} - \Delta \boldsymbol{E}_{trans}$ (kJ/mol)
X = N_2	−5.42	−4.35	−1.08
X = Ar	−3.73	−3.43	−0.30
X = Xe	−6.11	−6.13	+0.03

Table 4. Summary of the average binding energy of all optimized 1:1 complex of X…CH_3ONO, where X = N_2, Ar, or Xe.

	Average $\Delta \boldsymbol{E}$ of All Optimized X…*cis*-CH_3ONO (kJ/mol)	Average $\Delta \boldsymbol{E}$ of All Optimized X…*trans*-CH_3ONO (kJ/mol)	Average $\Delta \boldsymbol{E}_{cis} - \Delta \boldsymbol{E}_{trans}$ (kJ/mol)
X = N_2	−3.97	−3.36	−0.61
X = Ar	−2.37	−2.49	+0.12
X = Xe	−4.99	−4.76	−0.23

The results of the quantum chemistry calculations of the 1:1 van der Waals complexes show that there is preferential binding of the lowest energy rotational isomer—*cis*-CH_3ONO—when deposited with N_2, which we extend to provide understanding of the process of diffusion on a surface. Ar and Xe do not exhibit an energetic preference toward the *cis* or *trans* conformer, indicating that energetic arguments are not sufficient for rationalizing conformer enhancement upon deposition.

4. Discussion

The experimental observations in this paper indicate that *cis*-CH_3ONO becomes enriched in inert-gas matrices relative to gas-phase abundances. Not only is this enrichment observed in the matrix, but the degree of this enrichment was also demonstrated to vary as a function of matrix

https://doi.org/10.26434/chemrxiv-2023-4vtc9 **ORCID:** https://orcid.org/0000-0001-5960-056X Content not peer-reviewed by ChemRxiv. **License:** CC BY 4.0

host identity (N_2, Ar, and Xe) and—in the case of N_2—also depends on deposition angle. These observations are in contradiction to the conventional matrix-isolation assumption that gas phase abundances are transferred to the matrix phase upon deposition. To investigate the underlying chemical physics behind our observations, we turn to the literature on surface-mediated processes. In this section, we discuss how the effects of surface morphology and energetic stabilization contribute to the observed change in conformer abundance.

When gas-phase molecules are deposited perpendicular to a cold substrate (α = 0°), their probabilities of desorption and diffusion are decreased, compared to their probabilities when deposited at an angle. This is because in a perpendicular deposition scheme, kinetic energy transfers more efficiently from the incoming gas molecule to the matrix, speeding the cooling process.[68] When the angle of deposition deviates from normal to an oblique angle, there is an increase in the momentum component of the molecule parallel to the surface and concomitant decrease in its perpendicular momentum. Due to the decreased effectiveness of cooling, the parallel momentum component increases the timescale for surface diffusion and consequently increases the probability that the molecule desorbs from the surface into vacuum.[57,60,62] If the incoming molecules diffuse on the surface they can: (a) diffuse long enough for a fresh layer of incoming gases to cover them, (b) interact with surface deformities that aid in dissipating excess energy and cause the molecules to stick to the surface, (c) insert into a substitutional site, and/or (d) desorb into vacuum. While there is not extensive research on the surface morphology of inert-matrix samples during deposition, we endeavor to understand the effects of deposition conditions on the matrix-isolation dynamics through our experimental results.

To the authors' knowledge, there have not been experimental investigations into the effects of deposition angle on the surface structure of inert-gas matrices for the purposes of matrix-isolation. We therefore turn to the literature on the deposition dynamics of thin films, previously investigated via MD simulations, Monte Carlo (MC) simulations, and experiments. These published studies have revealed that changing the incident angle of deposition (at a constant incident energy) can have various effects on the formed thin film, altering such properties as the surface morphology, density, and sticking probability.[52,58,66,94] Mes-adi et al. showed using MD simulations that the OAD of Cu atoms exceeding 60° from the normal of a Si surface, can produce more voids and vacancies in a thin film, leading to rougher surface morphology than when deposited from 0° to 45°, which generates a more uniform and smooth surface.[95] This is corroborated by Zhu et al., using a MC-MD coupling method to show that the surface morphology was almost flat when Cu atoms were deposited with incident angles less than 45°.[96] Based on these two model studies depicting the growth of an atomic species deposited onto a flat surface, in combination with earlier simulations by Cruz and Lopez that used classical MD simulations to depict the slow-deposition of Ar at 10 K, we do not expect significant differences in the surface morphologies of the atomic matrices in this study (Ar and Xe) when the deposition angle is changed.

A limited number of simulation and experimental studies investigating the surface morphology of matrix-isolated N_2 have been performed. Experimental characterization studies of the crystal structure of N_2 indicate that there are three structural forms: α-N_2, β-N_2, or γ-N_2.[40,97] While the temperatures and pressures needed to form γ-N_2 are outside of the range of this experiment, both α-N_2 and β-N_2 packing motifs are possible when depositing a room-temperature gas phase mixture onto a 10 K substrate. As shown experimentally by Beker et al., through X-ray diffraction and IR spectroscopy, molecular N_2 deposited under matrix-isolation conditions forms a particularly porous surface due to the random orientation of N_2 molecules on the cold substrate.[98] As a result, incoming molecules used in the study (Ar and CH_4) were trapped easily in the large pores in the

https://doi.org/10.26434/chemrxiv-2023-4vtc9 **ORCID:** https://orcid.org/0000-0001-5960-056X Content not peer-reviewed by ChemRxiv. **License:** CC BY 4.0

N_2 layer. It has been noted, however, that high-level modeling specifically of the deposition process of matrix-isolated N_2 is currently unattainable based on inadequate documentation of the needed pair potential.[102] Based on the limited literature available, we predict that the surface roughness of N_2 increases with larger deposition angles. This increased surface roughness exhibits an increase in surface deformities and pockets for CH_3ONO trapping.

Experimental trends in the angular dependance of the sticking probability can vary greatly from system to system, as summarized in Kindt and Tully and references therein.[66] For example, CO deposited onto various substrates (Au, Pt, Cu, Ni) exhibit starkly different sticking probabilities as a function of incident angle deposition.[53,54,99,100] Currently, our experiment is not configured to determine the sticking probability of CH_3ONO onto various low-temperature matrices using a strategy such as the King and Wells technique.[101] However, such a technique would not provide conformer-specific sticking information needed for this study due to the lack of isomeric specificity in a commercial mass spectrometer. Future experiments are needed that can measure conformer-specific sticking probabilities to begin unraveling the competition between energetic and surface morphological effects on abundance changes during matrix deposition of CH_3ONO in N_2, Ar, and Xe, but these are outside the scope of the present study.

In Sections 3.2-3.3 we report a retention of the gas-phase conformer abundance when N_2:CH_3ONO is deposited normal to the surface while the *cis* conformer abundance is enhanced as the angle of deposition deviates from normal. When deposited normal to the surface, CH_3ONO cools rapidly and does not have sufficient time to diffuse and desorb, resulting in abundances that match those of the gas phase. When deposited at an angle, the momentum vector of CH_3ONO has a parallel component, enabling processes such as surface diffusion and desorption. Quantum chemistry calculations indicate that N_2:*cis*-CH_3ONO is energetically stabilized relative to *trans*:N_2. We therefore argue that when N_2:CH_3ONO is deposited at an angle, CH_3ONO does not cool rapidly enough to trap both conformers in their gas phase abundances. Instead, CH_3ONO undergoes processes like surface diffusion and desorption. During these processes, the larger energetic stabilization of *cis*:N_2 results in decreased desorption of *cis* compared to *trans*, leading to enhancement of the matrix-isolated *cis* conformer. Energetic stabilization of cis does not preclude enhancement of the cis abundance from surface morphology effects. However, further theoretical and experimental characterization of the angular dependence of N_2 matrix deposition is needed.

As reported in Sections 3.2-3.3, conformer abundances of CH_3ONO deposited in Ar indicate an enhancement of *cis* that does not change with deposition angle. Quantum chemistry calculations do not indicate strong energetic preference for *cis*:Ar or *trans*:Ar. As a result from the calculations, surface morphological effects are likely to contribute to the enhancement of the *cis* conformer. However, because we see no changes in *cis* enhancement with deposition angle, we conclude that surface morphologies do not change substantially with deposition angle. Contrary to the results in N_2, we see enhanced *cis* abundance even at perpendicular deposition angles. We thus conclude that CH_3ONO, even at perpendicular deposition, has sufficient time to diffuse and desorb at all angles studied, enabling the enhancement of *cis* due to trapping in surface pockets. We propose that the smaller van der Waals radius of the *cis* conformer enables enhanced trapping over the larger trans conformer, resulting in increased *cis* abundance in the matrices. However, we acknowledge that we cannot explicitly rule out that this initial enhancement of *cis*-CH_3ONO occurs during the gas-phase portion of the deposition process, since our effusive source is much further from the cold substrate (~8 cm) than previous studies (assumed to be on the millimeter to centimeter scale based on schematics), allowing for more collisions and/or other processes that

https://doi.org/10.26434/chemrxiv-2023-4vtc9 **ORCID:** https://orcid.org/0000-0001-5960-056X Content not peer-reviewed by ChemRxiv. **License:** CC BY 4.0

could enhance the lowest energy conformer,[102–107] although we believe it unlikely given the high isomerization barrier of this system.

In Section 3.2 we report the conformer abundances of CH_3ONO deposited in Xe, indicating a significant enhancement of *cis* at a deposition angle of $\alpha = 20°$. Quantum chemistry calculations, reported in Section 3.4 do not indicate that Xe binds preferentially to either the *cis* or *trans* conformer. We therefore explain the increased *cis* abundances in Xe as originating from surface morphological effects, as found for CH_3ONO:Ar. Because the literature on Xe matrix formation dynamics and surface morphologies is quite sparse, we cannot make predictions about the angular dependence of conformer abundances. We reiterate a need for future experimental and theoretical characterization of the surface formation dynamics, morphologies, and sticking coefficients between CH_3ONO and a Xe matrix.

5. Conclusion

Our experimental observations demonstrate an enhancement of the *cis* conformer abundance of CH_3ONO upon matrix isolation that has not been identified previously. Our systematic study of the angular and host dependances of the observed isomer abundances implicates gas/surface interactions during the deposition process as being responsible for this enhancement. We conclude that enhancement of the *cis* conformer is due to a competition between energetic stabilization of *cis* and enhanced surface trapping of *cis* due to its smaller van der Waals radius.

At oblique angles of deposition, the parallel momentum of the incoming CH_3ONO molecules enables increased diffusion on the surface compared to diffusion after perpendicular deposition. Increased time on the surface during diffusion leads to the increased likelihood that molecules can desorb into vacuum. However, due to preferential binding of a given conformer to N_2, suggested from the 1:1 complex results, we conclude that the enhancement of the lowest energy conformer—*cis*-CH_3ONO—is a result of a stronger binding interaction during the diffusion process. The binding interaction during diffusion will increase the likelihood that the preferential conformer remains on the surface long enough to become isolated, instead of being desorbed into vacuum. We conclude that, in addition to the energetic preference, the surface morphology of the N_2 matrix is highly sensitive to the deposition angle due to the random orientation of the diatomic molecule upon impact. The altered surface morphology with increased deposition angle enables longer CH_3ONO diffusion timescales, resulting in enhanced trapping of the smaller *cis* conformer and subsequent *cis* abundance enhancement.

Since there is no substantial preferential binding between the 1:1 conformers and Ar, we conclude that the global enrichment of *cis*-CH_3ONO is a result of enhanced *cis* trapping in surface pockets due to its smaller van der Waals radius compared to the *trans* conformer. We also demonstrated that the *cis* abundance enhancement does not change with deposition angle, concluding that the surface morphology of the Ar matrix does not change significantly with deposition angle.

Quantum chemistry calculations of the 1:1 CH_3ONO:Xe complex suggest that there is no substantial energetic preference between the *cis* or *trans* conformers. As in the case of Ar, we conclude that surface morphology effects enable enhanced trapping of the *cis* conformer.

We observe that different bath gases and deposition angles create different dynamical matrix surfaces, changing the conformer abundances of rotational isomers of CH_3ONO compared to the gas phase. We conclude that a competition between energetic effects and surface morphological effects dictate changes in these abundances. Our results highlight the necessity for detailed characterization of conformer abundances in matrix-isolated systems. These results also emphasize

https://doi.org/10.26434/chemrxiv-2023-4vtc9 **ORCID:** https://orcid.org/0000-0001-5960-056X Content not peer-reviewed by ChemRxiv. **License:** CC BY 4.0

the need for future experimental and theoretical studies of the dynamics of inert gas matrix deposition, including quantification of the effects of local energetic stabilization and enhanced surface trapping of rotational conformers.

Author Declarations

Corresponding Author
LMM *lmmccas@sandia.gov, LGD *ldodson@umd.edu

Acknowledgements
Acknowledgement is made to the donors of the American Chemical Society Petroleum Research Fund for support of this research. Additional support for this work was provided by a University of Maryland startup grant. L.M.M. was funded by the Division of Chemical Sciences, Geosciences and Biosciences, Office of Basic Energy Sciences (BES), U.S. Department of Energy (USDOE). This article has been co-authored by an employee of National Technology Engineering Solutions of Sandia. Sandia National Laboratories is a multi-mission laboratory managed and operated by National Technology & Engineering Solutions of Sandia, LLC (NTESS), a wholly owned subsidiary of Honeywell International Inc., for the U.S. Department of Energy's National Nuclear Security Administration (DOE/NNSA) under contract DE-NA0003525. The employee, not NTESS, owns the right, title and interest in and to the written work and is responsible for its contents. Any subjective views or opinions that might be expressed in the written work do not necessarily represent the views of the U.S. Government. The publisher acknowledges that the U.S. Government retains a non-exclusive, paid-up, irrevocable, world-wide license to publish or reproduce the published form of this written work or allow others to do so, for U.S. Government purposes. The DOE will provide public access to results of federally sponsored research in accordance with the DOE Public Access Plan.

Supplemental Material
The supporting information contains detailed explanation of conformer abundance determination using integrated absorbance, gas-phase spectra of Ar:CH_3ONO and N_2:CH_3ONO, full spectral range matrix-isolated infrared spectra of X:CH_3ONO (X = N_2, Ar, Xe), effusive source characterization, matrix-isolated spectra of varying deposition angles for Ar:CH_3ONO and N_2:CH_3ONO.

Conflict of Interest
The authors have no conflicts to disclose.

Author Contributions
Emily K. Hockey: Conceptualization (equal); Data Curation (lead); Investigation (equal); Formal Analysis (equal); Methodology (lead); Validation (equal); Visualization (lead); Writing/Original Draft Preparation (lead); Writing/Reviewing & Editing (equal). **Nathan McLane**: Conceptualization (equal); Investigation (equal); Formal Analysis (equal); Validation (equal); Writing/Reviewing & Editing (equal). **Korina Vlahos**: Conceptualization (supporting); Formal Analysis (supporting). **Laura M. McCaslin**: Computations (lead); Formal Analysis (supporting); Writing/Review & Editing (supporting). **Leah G. Dodson**: Conceptualization (equal); Formal

https://doi.org/10.26434/chemrxiv-2023-4vtc9 **ORCID:** https://orcid.org/0000-0001-5960-056X Content not peer-reviewed by ChemRxiv. **License:** CC BY 4.0

Analysis (equal); Funding Acquisition (lead); Project Administration (lead); Supervision (lead); Validation (equal); Writing/Review & Editing (equal).

Data Availability

The data that support the findings of this study are available from the corresponding author upon reasonable request.

References

[1] L. D'Or, and P. Tarte, "Rotational Isomerism in Nitrous Acid and Alkyl Nitrites," The Journal of Chemical Physics **19**(8), 1064–1065 (1951).

[2] P. Tarte, "Recherches spectroscopiques sur les esters de l'acide nitreux," Bull. Soc. Chim. Belges **60**(3–4), 227–239 (1951).

[3] P. Tarte, "Rotational Isomerism as a General Property of Alkyl Nitrites," The Journal of Chemical Physics **20**(10), 1570–1575 (1952).

[4] H.W. Brown, and G.C. Pimentel, "Photolysis of Nitromethane and of Methyl Nitrite in an Argon Matrix; Infrared Detection of Nitroxyl, HNO," The Journal of Chemical Physics **29**(4), 883–888 (1958).

[5] L.H. Piette, and W.A. Anderson, "Potential Energy Barrier Determinations for Some Alkyl Nitrites by Nuclear Magnetic Resonance," The Journal of Chemical Physics **30**(4), 899–908 (1959).

[6] P. Gray, and M.J. Pearson, "Dielectric constant measurements, effective dipole moments and rotational isomer abundances in alkyl nitrites," Trans. Faraday Soc. **59**, 347 (1963).

[7] Klaboe, P., Jones, Derek, and Lippincott, E.R, "The infrared spectra and the rotational isomerism of methyl and ethyl nitrite," Spectrochimica Acta Part A: Molecular Spectroscopy **23**(12), 2957–2971 (1967).

[8] Napier, I.M and Norrish, R.G. W, "The photolysis and pyrolysis of nitromethane and methyl nitrite," Proceedings of the Royal Society A, 317–336 (1967).

[9] J.F. Ogilvie, "Vibrational assignments for methyl nitrite rotamers," J. Chem. Soc., Chem. Commun. (13), 450 (1973).

[10] Felder, Peter and Gunthard, HsH, "Freezing of Internal Rotation Temperature in a Supersonic Jet Detected by Matrix IR Spectroscopy," Chemical Physics Letters **66**(2), (1979).

[11] P.H. Turner, M.J. Corkill, and A.Peter. Cox, "Microwave spectra and structures of cis- and trans-methyl nitrite. Methyl barrier in trans-methyl nitrite," J. Phys. Chem. **83**(11), 1473–1482 (1979).

[12] S.H. Bauer, and N.S. True, "Kinetics of the syn → anti isomerization of methyl nitrite," J. Phys. Chem. **84**(20), 2507–2516 (1980).

[13] Ghosh, Pramid and Gunthard, HsH, "Cis and trans methyl nitrite: Gas phase i.r. spectra, band envelope analysis, hot band progressions and assignments," Spectrochimica Acta Part A: Molecular Spectroscopy **37**(5), 347–363 (1981).

[14] P.N. Ghosh, and Hs.H. Günthard, "Infrared matrix spectra, normal coordinate analysis and valence force field of six isotopomers of methyl nitrite," Spectrochimica Acta Part A: Molecular Spectroscopy **37**(12), 1055–1065 (1981).

[15] P. Felder, T.-K. Ha, A.M. Dwivedi, and Hs.H. Günthard, "Cis and trans methyl nitrite: Effusive molecular beam i.r. matrix spectra; thermodynamics and ab initio calculation of the cis-trans interconversion," Spectrochimica Acta Part A: Molecular Spectroscopy **37**(5), 337–345 (1981).

https://doi.org/10.26434/chemrxiv-2023-4vtc9 **ORCID:** https://orcid.org/0000-0001-5960-056X Content not peer-reviewed by ChemRxiv. **License:** CC BY 4.0

[16] M.E. Jacox, and F.L. Rook, "Photodecomposition of methyl nitrite trapped in solid argon," J. Phys. Chem. **86**(15), 2899–2904 (1982).
[17] F.L. Rook, and M.E. Jacox, "The vibrational spectra of methyl and methyl-d3 nitrite," Journal of Molecular Spectroscopy **93**(1), 101–116 (1982).
[18] F.L. Rook, "Preparation, vapor pressure, and infrared spectrum of methyl nitrite," Journal of Chemical & Engineering Data **27**(1), 72–73 (1982).
[19] Felder, Peter and Gunthard, HsH, "Conformational Interconversions in Supersonic Jets: Matrix IR Spectroscopy and Model Calculations," Chemical Physics **71**, 9–25 (1982).
[20] J.P. Chauvel, and N.S. True, "Phase effects on conformational equilibriums. Nuclear magnetic resonance studies of methyl nitrite," J. Phys. Chem. **87**(9), 1622–1625 (1983).
[21] Barnes, A J, "Matrix Isolation Vibrational Spectroscopy as a Tool for Studying Conformational Isomerism," Journal of Molecular Structure **113**, 161–174 (1984).
[22] J.P. Chauvel, and N.S. True, "Conformational kinetics of methyl nitrite. II. Phase dependence of kinetic parameters," The Journal of Chemical Physics **80**(8), 3561–3568 (1984).
[23] C.B. Conboy, J.P. Chauvel, P.O. Moreno, N.S. True, and C.M. Ott, "Gas- and liquid-phase proton NMR study of the syn-anti conformer equilibrium of ethyl, n-propyl, isopropyl, n-butyl, isobutyl, tert-butyl and neopentyl nitrite," J. Phys. Chem. **90**(18), 4353–4358 (1986).
[24] B.J. Van der Veken, R. Maas, G.A. Guirgis, H.D. Stidham, T.G. Sheehan, and J.R. Durig, "Infrared spectrum, ab initio calculations, barriers to internal rotation and structural parameters for methyl nitrite," J. Phys. Chem. **94**(10), 4029–4039 (1990).
[25] M. Hippler, and J. Pfab, "Electronic Absorption Spectrum of Methyl Nitrite in the Near-ultraviolet," J. Chem. Soc. Faraday Trans. **88**(14), 2109–2110 (1992).
[26] M. Bodenbinder, S.E. Ulic, and H. Willner, "A Gas-Phase and Matrix Isolation Study of the Equilibrium CH3ONO (cis) ↔ CH3ONO (trans) by FTIR Spectroscopy," The Journal of Physical Chemistry **98**(26), 6441–6444 (1994).
[27] J.M. Engert, and B. Dick, "Measurement and assignment of the vibrationally resolved UV absorption spectrum of syn-methyl nitrite isolated in an argon matrix at 12 K," Chemical Physics Letters **299**(5), 423–429 (1999).
[28] B.J. van der Veken, and W.A. Herrebout, "Conformational Characteristics of Methyl Nitrite: A Cryospectroscopic Study," J. Phys. Chem. A **105**(30), 7198–7204 (2001).
[29] L.M. Goss, C.D. Mortensen, and T.A. Blake, "Rotationally resolved spectroscopy of the ν8 band of cis-methyl nitrite," Journal of Molecular Spectroscopy **225**(2), 182–188 (2004).
[30] P. Maksyutenko, M. Förstel, P. Crandall, B.-J. Sun, M.-H. Wu, A.H.H. Chang, and R.I. Kaiser, "An isomer-specific study of solid nitromethane decomposition pathways – Detection of aci-nitromethane (H2CNO(OH)) and nitrosomethanol (HOCH2NO) intermediates," Chemical Physics Letters **658**, 20–29 (2016).
[31] P.M. Coulter, M.P. Grubb, and A.J. Orr-Ewing, "Conformer-specific geminate recombination following methyl nitrite photolysis in solution," Chemical Physics Letters **683**, 416–420 (2017).
[32] S.K. Singh, and R.I. Kaiser, "A vacuum ultraviolet photoionization study on the isomerization, decomposition, and molecular mass growth processes in solid nitromethane (CH3NO2)," Chemical Physics Letters **766**, 138343 (2021).
[33] T. Chiba, "Studies on Molecular Structure by the Measurement of the Dielectric Constants of Gases. III. The Dipole Moment and the Structure of Alkyl Nitrites," BCSJ **28**(7), 505–509 (1955).
[34] Farnell, L and Ogilvie, J.F, "Quantum chemical computations on rotational isomers of hydrogen nitrite and nitritomethane," Proc. R. Soc. Lond. A **381**(1781), 443–455 (1982).

https://doi.org/10.26434/chemrxiv-2023-4vtc9 **ORCID:** https://orcid.org/0000-0001-5960-056X Content not peer-reviewed by ChemRxiv. **License:** CC BY 4.0

[35] M.L. McKee, "Ab initio study of rearrangements on the nitromethane potential energy surface," J. Am. Chem. Soc. **108**(19), 5784–5792 (1986).
[36] J.A. Darsey, and D.L. Thompson, "Ab initio molecular orbital calculation of the methyl nitrite syn-anti isomerization potential," Chemical Physics Letters **145**(6), 523–528 (1988).
[37] A. Preiskorn, and D.L. Thompson, "Cis–trans isomerization of methyl nitrite," The Journal of Chemical Physics **91**(4), 2299–2307 (1989).
[38] E. Martínez-Núñez, and S.A. Vázquez, "Further studies of the methyl nitrite cis→trans isomerization," The Journal of Chemical Physics **107**(14), 5393–5405 (1997).
[39] A. Dey, R. Fernando, C. Abeysekera, Z. Homayoon, J.M. Bowman, and A.G. Suits, "Photodissociation dynamics of nitromethane and methyl nitrite by infrared multiphoton dissociation imaging with quasiclassical trajectory calculations: Signatures of the roaming pathway," The Journal of Chemical Physics **140**(5), 054305 (2014).
[40] Andrews, Lester and Moskovits, Martin, *Chemistry and Physics of Matrix-Isolated Species* (Elsevier Science Publisher B.V, 1989).
[41] Dunkin, Ian R., *Matrix-Isolation Techniques: A Practical Approach* (Oxford University Press Inc, New York, USA, 1998).
[42] S. Kudoh, M. Takayanagi, and M. Nakata, "Conformational cooling in a supersonic jet of 1,2-dichloroethane studied by matrix isolation infrared spectroscopy," Chemical Physics Letters **296**(3–4), 329–334 (1998).
[43] L. Khriachtchev, J. Lundell, E. Isoniemi, and M. Räsänen, "HONO in solid Kr: Site-selective *trans* ↔ *cis* isomerization with narrow-band infrared radiation," The Journal of Chemical Physics **113**(10), 4265–4273 (2000).
[44] I.D. Reva, S.V. Ilieva, and R. Fausto, "Conformational isomerism in methyl cyanoacetate: A combined matrix-isolation infrared spectroscopy and molecular orbital study," Phys. Chem. Chem. Phys. **3**(19), 4235–4241 (2001).
[45] M. Pettersson, E.M.S. Maçôas, L. Khriachtchev, J. Lundell, R. Fausto, and M. Räsänen, "*Cis* → *trans* conversion of formic acid by dissipative tunneling in solid rare gases: Influence of environment on the tunneling rate," The Journal of Chemical Physics **117**(20), 9095–9098 (2002).
[46] A. Borba, A. Gómez-Zavaglia, and R. Fausto, "Conformational cooling and conformation selective aggregation in dimethyl sulfite isolated in solid rare gases," Journal of Molecular Structure **794**(1–3), 196–203 (2006).
[47] M.T.S. Rosado, A.J. Lopes Jesus, I.D. Reva, R. Fausto, and J.S. Redinha, "Conformational Cooling Dynamics in Matrix-Isolated 1,3-Butanediol," The Journal of Physical Chemistry A **113**(26), 7499–7507 (2009).
[48] I.D. Reva, S.G. Stepanian, L. Adamowicz, and R. Fausto, "Missing conformers. Comparative study of conformational cooling in cyanoacetic acid and methyl cyanoacetate isolated in low temperature inert gas matrixes," Chemical Physics Letters **374**(5–6), 631–638 (2003).
[49] R.S. Ruoff, T.D. Klots, T. Emilsson, and H.S. Gutowsky, "Relaxation of conformers and isomers in seeded supersonic jets of inert gases," The Journal of Chemical Physics **93**(5), 3142–3150 (1990).
[50] C. Cabezas, J.-C. Guillemin, and Y. Endo, "Conformational preferences of Criegee intermediates: Isopropyl substituted carbonyl oxide," The Journal of Chemical Physics **149**(8), 084309 (2018).

https://doi.org/10.26434/chemrxiv-2023-4vtc9 **ORCID:** https://orcid.org/0000-0001-5960-056X Content not peer-reviewed by ChemRxiv. **License:** CC BY 4.0

[51] A.Yu. Ivanov, and S.G. Stepanian, "Molecular structure and vibrational spectra of isolated nucleosides at low temperatures (Review article)," Low Temperature Physics **47**(3), 181–198 (2021).
[52] M.J. Cardillo, "Gas-Surface Interactions Studied with Molecular Beam Techniques," Annu. Rev. Phys. Chem. **32**(1), 331–357 (1981).
[53] M. D'Evelyn P., H.-P. Steinrück, and R.J. Madix, "Precursors and Trapping in the Molecular Chemisorption of CO on Ni(100)," Surface Science **180**, 47–76 (1987).
[54] J. Harris, and A.C. Luntz, "Sticking and scattering in the molecular chemisorption regime: CO on Pt(111)," The Journal of Chemical Physics **91**(10), 6421–6428 (1989).
[55] C.T. Rettner, D.S. Bethune, and D.J. Auerbach, "Effect of incidence energy and angle on the adsorption probability of Xe on Pt(111): Energy–angle scaling relations," The Journal of Chemical Physics **91**(3), 1942–1943 (1989).
[56] C. Arumainayagam R., R.J. Madix, and M. McMaster C., "Trapping Dynamics of Xenon on Pt(111)," Surface Science **226**, 180–190 (1990).
[57] L.A. DeLouise, "Trapping dynamics in reactive gas/surface scattering: importance of parallel momentum accommodation," Chemical Physics Letters **180**(3), 149–155 (1991).
[58] K.D. Rendulic, "Sticking and desorption: a review," Surface Science **272**(1–3), 34–44 (1992).
[59] J.K. Brown, and A.C. Luntz, "NO sticking on a Pt(111) surface," Chemical Physics Letters **204**(5–6), 451–454 (1993).
[60] M. McMaster C., S. Schroeder, and Madix, Robert J., "Molecular propane adsorption dynamics on Pt(llO)-(1 x 2)," Surface Science **297**, 253–271 (1993).
[61] S. Schroeder, M. McMaster C., J.A. Stinnett, and Madix, Robert J., "Surface corrugation effects on the adsorption dynamics of xenon on Pt(1lO)-(1 X 2)," Surface Science Letters **297**(3), L148–L155 (1993).
[62] J.A. Stinnett, M. McMaster C., S. Schroeder, and Madix, Robert J., "Surface microstructure effects: molecular ethane adsorption dynamics on Pt(ll0)-(1 x 2)," Surface Science **365**, 683–700 (1996).
[63] J.F. Weaver, and R.J. Madix, "Trapping dynamics of isobutane, *n* -butane, and neopentane on Pt(111): Effects of molecular weight and structure," The Journal of Chemical Physics **110**(21), 10585–10598 (1999).
[64] C.T. Reeves, B.A. Ferguson, C.B. Mullins, G.O. Sitz, B.A. Helmer, and D.B. Graves, "Trapping dynamics of ethane on Si(100)-(2×1): Molecular beam experiments and molecular dynamics simulations," The Journal of Chemical Physics **111**(16), 7567–7575 (1999).
[65] A. Al-Halabi, A.W. Kleyn, and G.J. Kroes, "Sticking of HCl to ice at hyperthermal energies: Dependence on incidence energy, incidence angle, and surface temperature," The Journal of Chemical Physics **115**(1), 482–491 (2001).
[66] J.T. Kindt, and J.C. Tully, "Dynamical corrugation: simulations of the sticking of CO on Cu(100)," Surface Science **477**(2–3), 149–162 (2001).
[67] G.A. Kimmel, K.P. Stevenson, Z. Dohnálek, R.S. Smith, and B.D. Kay, "Control of amorphous solid water morphology using molecular beams. I. Experimental results," The Journal of Chemical Physics **114**(12), 5284–5294 (2001).
[68] E.R. Batista, P. Ayotte, A. Bilić, B.D. Kay, and H. Jónsson, "What Determines the Sticking Probability of Water Molecules on Ice?," Phys. Rev. Lett. **95**(22), 223201 (2005).
[69] S.E. Bisschop, H.J. Fraser, K.I. Öberg, E.F. Van Dishoeck, and S. Schlemmer, "Desorption rates and sticking coefficients for CO and N_2 interstellar ices," A&A **449**(3), 1297–1309 (2006).

https://doi.org/10.26434/chemrxiv-2023-4vtc9 **ORCID:** https://orcid.org/0000-0001-5960-056X Content not peer-reviewed by ChemRxiv. **License:** CC BY 4.0

[70] J. Ceponkus, P. Uvdal, and B. Nelander, "Complex Formation of Small Molecules during Isolation in Low Temperature Matrices: Water Dimers in *p* -H $_2$ and Ne Matrices," J. Phys. Chem. A **114**(25), 6829–6831 (2010).
[71] K.D. Gibson, D.R. Killelea, H. Yuan, J.S. Becker, and S.J. Sibener, "Determination of the sticking coefficient and scattering dynamics of water on ice using molecular beam techniques," The Journal of Chemical Physics **134**(3), 034703 (2011).
[72] R.S. Thompson, M.R. Brann, and S.J. Sibener, "Sticking Probability of High-Energy Methane on Crystalline, Amorphous, and Porous Amorphous Ice Films," J. Phys. Chem. C **123**(29), 17855–17863 (2019).
[73] M.R. Brann, R.S. Thompson, and S.J. Sibener, "Reaction Kinetics and Influence of Film Morphology on the Oxidation of Propene Thin Films by O(^{3} P) Atomic Oxygen," J. Phys. Chem. C **124**(13), 7205–7215 (2020).
[74] M.R. Brann, S.P. Hansknecht, X. Ma, and S.J. Sibener, "Differential Condensation of Methane Isotopologues Leading to Isotopic Enrichment under Non-equilibrium Gas–Surface Collision Conditions," J. Phys. Chem. A **125**(42), 9405–9413 (2021).
[75] M.R. Brann, S.P. Hansknecht, M. Muir, and S.J. Sibener, "Acetone–Water Interactions in Crystalline and Amorphous Ice Environments," J. Phys. Chem. A **126**(17), 2729–2738 (2022).
[76] E.K. Hockey, K. Vlahos, T. Howard, J. Palko, and L.G. Dodson, "Weakly Bound Complex Formation between HCN and CH_3Cl: A Matrix-Isolation and Computational Study," J. Phys. Chem. A **126**(20), 3110–3123 (2022).
[77] E. Epifanovsky, A.T.B. Gilbert, X. Feng, J. Lee, Y. Mao, N. Mardirossian, P. Pokhilko, A.F. White, M.P. Coons, A.L. Dempwolff, Z. Gan, D. Hait, P.R. Horn, L.D. Jacobson, I. Kaliman, J. Kussmann, A.W. Lange, K.U. Lao, D.S. Levine, J. Liu, S.C. McKenzie, A.F. Morrison, K.D. Nanda, F. Plasser, D.R. Rehn, M.L. Vidal, Z.-Q. You, Y. Zhu, B. Alam, B.J. Albrecht, A. Aldossary, E. Alguire, J.H. Andersen, V. Athavale, D. Barton, K. Begam, A. Behn, N. Bellonzi, Y.A. Bernard, E.J. Berquist, H.G.A. Burton, A. Carreras, K. Carter-Fenk, R. Chakraborty, A.D. Chien, K.D. Closser, V. Cofer-Shabica, S. Dasgupta, M. de Wergifosse, J. Deng, M. Diedenhofen, H. Do, S. Ehlert, P.-T. Fang, S. Fatehi, Q. Feng, T. Friedhoff, J. Gayvert, Q. Ge, G. Gidofalvi, M. Goldey, J. Gomes, C.E. González-Espinoza, S. Gulania, A.O. Gunina, M.W.D. Hanson-Heine, P.H.P. Harbach, A. Hauser, M.F. Herbst, M.H. Vera, M. Hodecker, Z.C. Holden, S. Houck, X. Huang, K. Hui, B.C. Huynh, M. Ivanov, Á. Jász, H. Ji, H. Jiang, B. Kaduk, S. Kähler, K. Khistyaev, J. Kim, G. Kis, P. Klunzinger, Z. Koczor-Benda, J.H. Koh, D. Kosenkov, L. Koulias, T. Kowalczyk, C.M. Krauter, K. Kue, A. Kunitsa, T. Kus, I. Ladjánszki, A. Landau, K.V. Lawler, D. Lefrancois, S. Lehtola, R.R. Li, Y.-P. Li, J. Liang, M. Liebenthal, H.-H. Lin, Y.-S. Lin, F. Liu, K.-Y. Liu, M. Loipersberger, A. Luenser, A. Manjanath, P. Manohar, E. Mansoor, S.F. Manzer, S.-P. Mao, A.V. Marenich, T. Markovich, S. Mason, S.A. Maurer, P.F. McLaughlin, P. Morgante, J.W. Mullinax, K.J. Oosterbaan, G. Paran, A.C. Paul, S.K. Paul, F. Pavos, E.I. Proynov, Á. Rák, E. Ramos-Cordoba, B. Rana, A.E. Rask, A. Rettig, R.M. Richard, F. Rob, E. Rossomme, T. Scheele, M. Scheurer, M. Schneider, N. Sergueev, S.M. Sharada, W. Skomorowski, D.W. Small, C.J. Stein, Y.-C. Su, E.J. Sundstrom, Z. Tao, J. Thirman, G.J. Tornai, T. Tsuchimochi, N.M. Tubman, S.P. Veccham, O. Vydrov, J. Wenzel, J. Witte, A. Yamada, K. Yao, S. Yeganeh, S.R. Yost, A. Zech, I.Y. Zhang, X. Zhang, Y. Zhang, D. Zuev, A. Aspuru-Guzik, and A.T. Bell, "Software for the frontiers of quantum chemistry: An overview of developments in the Q-Chem 5 package," The Journal, (2023).
[78] A.D. Becke, "Density-functional thermochemistry. III. The role of exact exchange," The Journal of Chemical Physics **98**(7), 5648–5652 (1993).

https://doi.org/10.26434/chemrxiv-2023-4vtc9 **ORCID:** https://orcid.org/0000-0001-5960-056X Content not peer-reviewed by ChemRxiv. **License:** CC BY 4.0

[79] P.J. Stephens, F.J. Devlin, C.F. Chabalowski, and M.J. Frisch, "Ab Initio Calculation of Vibrational Absorption and Circular Dichroism Spectra Using Density Functional Force Fields," J. Phys. Chem. **98**(45), 11623–11627 (1994).
[80] S. Grimme, S. Ehrlich, and L. Goerigk, "Effect of the damping function in dispersion corrected density functional theory," J. Comput. Chem. **32**(7), 1456–1465 (2011).
[81] T.H. Dunning, "Gaussian basis sets for use in correlated molecular calculations. I. The atoms boron through neon and hydrogen," The Journal of Chemical Physics **90**(2), 1007–1023 (1989).
[82] D.E. Woon, and T.H. Dunning, "Gaussian basis sets for use in correlated molecular calculations. III. The atoms aluminum through argon," The Journal of Chemical Physics **98**(2), 1358–1371 (1993).
[83] K.A. Peterson, D. Figgen, E. Goll, H. Stoll, and M. Dolg, "Systematically convergent basis sets with relativistic pseudopotentials. II. Small-core pseudopotentials and correlation consistent basis sets for the post- *d* group 16–18 elements," The Journal of Chemical Physics **119**(21), 11113–11123 (2003).
[84] K. Raghavachari, G.W. Trucks, J.A. Pople, and M. Head-Gordon, "A fifth-order perturbation comparison of electron correlation theories," Chemical Physics Letters **157**(6), 479–483 (1989).
[85] R.J. Bartlett, J.D. Watts, S.A. Kucharski, and J. Noga, "Non-iterative fifth-order triple and quadruple excitation energy corrections in correlated methods," Chemical Physics Letters **165**(6), 513–522 (1990).
[86] Y.-F. Lee, W.-T. Chou, B.A. Johnson, D.P. Tabor, E.L. Sibert, and Y.-P. Lee, "Infrared absorption of CH3O and CD3O radicals isolated in solid para-H2," Journal of Molecular Spectroscopy **310**, 57–67 (2015).
[87] M. Kasha, "Collisional Perturbation of Spin-Orbital Coupling and the Mechanism of Fluorescence Quenching. A Visual Demonstration of the Perturbation," The Journal of Chemical Physics **20**(1), 71–74 (1952).
[88] S.N. Foner, E.L. Cochran, V.A. Bowers, and C.K. Jen, "Multiple Trapping Sites for Hydrogen Atoms in Rare Gas Matrices," The Journal of Chemical Physics **32**(4), 963–971 (1960).
[89] R. Pellow, and M. Vala, "The external heavy atom effect: Theory of spin–orbit coupling of alkali and noble metals in rare gas matrices," The Journal of Chemical Physics **90**(10), 5612–5621 (1989).
[90] Akai, Nobuyuki, Takayanagi, Masao, and Nakata, Munetaka, "Cis–trans isomerization equilibrium in hydroquinone in low-temperature argon and xenon matrices studied by FTIR spectroscopy," CHEMICAL PHYSICS LETTERS (356), 133–139 (2002).
[91] A. Kyrychenko, and J. Waluk, "Molecular dynamics simulations of matrix deposition. I. Site structure analysis for porphyrin in argon and xenon," The Journal of Chemical Physics **119**(14), 7318–7327 (2003).
[92] A. Kyrychenko, A. Gorski, and J. Waluk, "Molecular dynamics and density functional theory simulations of matrix deposition. II. Absolute site structure assignment for porphyrin in xenon," The Journal of Chemical Physics **121**(23), 12017–12025 (2004).
[93] A. Kyrychenko, and J. Waluk, "Molecular dynamics simulations of matrix deposition. III. Site structure analysis for porphycene in argon and xenon," The Journal of Chemical Physics **123**(6), 064706 (2005).
[94] A. Barranco, A. Borras, A.R. Gonzalez-Elipe, and A. Palmero, "Perspectives on oblique angle deposition of thin films: From fundamentals to devices," Progress in Materials Science **76**, 59–153 (2016).

https://doi.org/10.26434/chemrxiv-2023-4vtc9 **ORCID:** https://orcid.org/0000-0001-5960-056X Content not peer-reviewed by ChemRxiv. **License:** CC BY 4.0

[95] H. Mes-adi, K. Saadouni, and M. Mazroui, "Effect of incident angle on the microstructure proprieties of Cu thin film deposited on Si (001) substrate," Thin Solid Films **721**, 138553 (2021).
[96] G. Zhu, M. Han, B. Xiao, and Z. Gan, "Influence of Sputtering Pressure on the Micro-Topography of Sputtered Cu/Si Films: Integrated Multiscale Simulation," Processes **11**(6), 1649 (2023).
[97] T.A. Scott, "Solid and liquid nitrogen," Physics Reports **27**(3), 89–157 (1976).
[98] A. Becker, W. Langel, S. Maass, and E. Knoezinger, "Structure and morphology of gas-phase-deposited molecular nitrogen," J. Phys. Chem. **97**(21), 5525–5529 (1993).
[99] C.T. Rettner, "The search for direct vibrational excitation in gas–surface collisions of CO with Au(111)," The Journal of Chemical Physics **99**(7), 5481–5489 (1993).
[100] B.E. Hayden, and D.C. Godfrey, "Molecular Beam Scattering of CO from Cu(110): The Effect of Incident Translational Energy," Journal of Electron Spectroscopy and Related Phenomena **45**, 351–359 (1987).
[101] D.A. King, and M.G. Wells, "Molecular beam investigation of adsorption kinetics on bulk metal targets: Nitrogen on tungsten," Surface Science **29**(2), 454–482 (1972).
[102] U. Erlekam, M. Frankowski, G. von Helden, and G. Meijer, "Cold collisions catalyse conformational conversion," Phys. Chem. Chem. Phys. **9**(28), 3786 (2007).
[103] T.N. Wassermann, and M.A. Suhm, "Ethanol Monomers and Dimers Revisited: A Raman Study of Conformational Preferences and Argon Nanocoating Effects," J. Phys. Chem. A **114**(32), 8223–8233 (2010).
[104] W.Y. Sohn, M. Kim, S.-S. Kim, Y.D. Park, and H. Kang, "Solvent-assisted conformational isomerization and the conformationally-pure REMPI spectrum of 3-aminophenol," Phys. Chem. Chem. Phys. **13**(15), 7037 (2011).
[105] I. Kosendiak, J.M.E. Ahokas, J. Krupa, J. Lundell, and M. Wierzejewska, "Complexes of Glycolic Acid with Nitrogen Isolated in Argon Matrices. I. Structures and Thermal Effects," Molecules **24**(18), 3262 (2019).
[106] M. Lange, E. Sennert, and M.A. Suhm, "London Dispersion-Assisted Low-Temperature Gas Phase Synthesis of Hydrogen Bond-Inserted Complexes," Synlett **33**(20), 2004–2008 (2022).
[107] D.B. Abdallah, M.M.A. Mogren, S.D.A.A. Harbi, M.S.A. Salhi, and M. Hochlaf, "Collision excitation of nitrous acid (HONO) by helium: isomerization effect," Monthly Notices of the Royal Astronomical Society **521**(3), 4162–4172 (2023).

https://doi.org/10.26434/chemrxiv-2023-4vtc9 **ORCID:** https://orcid.org/0000-0001-5960-056X Content not peer-reviewed by ChemRxiv. **License:** CC BY 4.0

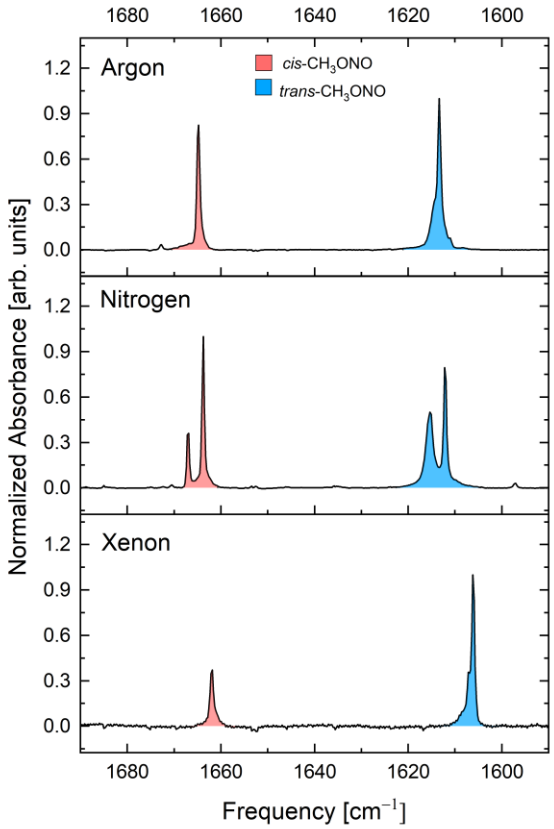

Fig. 5. Normalized matrix-isolated infrared spectra of the region corresponding to the ν_3 transition of CH_3ONO (1690–1590 cm^{-1}), shown for different low-temperature matrices. The deposition angle was fixed at $\alpha = 20°$ and the pre-mixed concentration remained constant at 500:1 X:CH_3ONO, where X = N_2 (top), Ar (middle), or Xe (bottom). The spectra have been color-coded showing regions assigned to the *cis* (blue) and *trans* (pink) conformers.

https://doi.org/10.26434/chemrxiv-2023-4vtc9 **ORCID:** https://orcid.org/0000-0001-5960-056X Content not peer-reviewed by ChemRxiv. **License:** CC BY 4.0

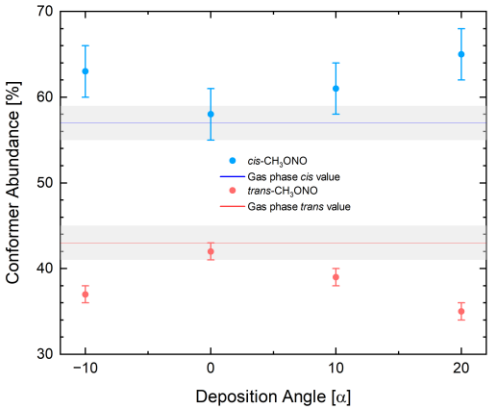

Fig. 6. Conformer abundance of matrix-isolated CH_3ONO in N_2 as a function of deposition angle (α) of the *cis* (blue) and *trans* (pink) ν_3 transition of 500:1 N_2:CH_3ONO observed between 1690–1590 cm^{-1}. The blue and red solid lines represent the gas-phase conformer abundance of 57 ± 2% to 43 ± 2%, where the gas-phase abundance errors are represented in shaded grey.

https://doi.org/10.26434/chemrxiv-2023-4vtc9 **ORCID:** https://orcid.org/0000-0001-5960-056X Content not peer-reviewed by ChemRxiv. **License:** CC BY 4.0

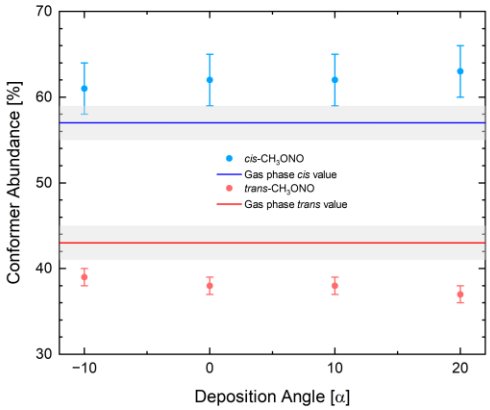

Fig. 7. Conformer abundance of matrix-isolated CH_3ONO in Ar as a function of deposition angle (α) of the *cis* (blue) and *trans* (pink) ν_3 transition of 500:1 Ar:CH_3ONO observed between 1690–1590 cm^{-1}. The blue and red solid lines represent the gas-phase conformer abundance of 57 ± 2% to 43 ± 2%, where the gas-phase abundance uncertainty is represented in shaded grey.

https://doi.org/10.26434/chemrxiv-2023-4vtc9 **ORCID:** https://orcid.org/0000-0001-5960-056X Content not peer-reviewed by ChemRxiv. **License:** CC BY 4.0

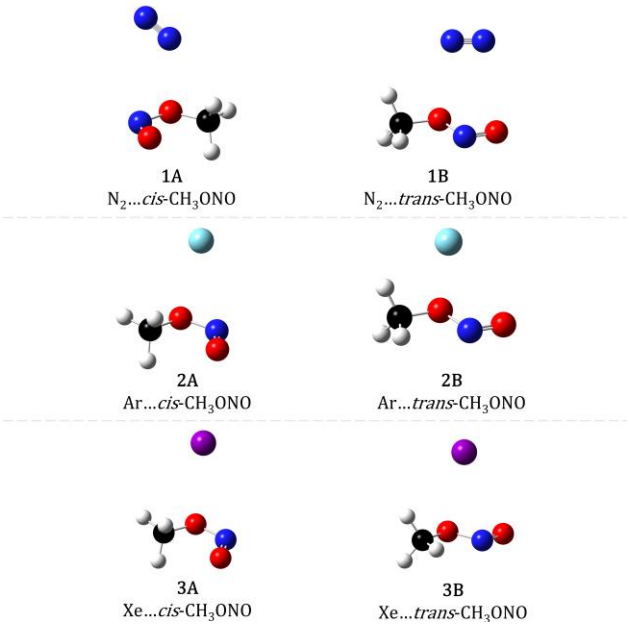

Fig. 8. Structural minima for 1:1 complexes of X…CH_3ONO, where X = N_2 (1A and 1B), Ar (2A and 2B) found at the B3LYP-D3/cc-pVDZ level of theory for structures containing N_2 and Ar. Structural minima for 1:1 complexes of X…CH_3ONO where X = Xe (3A and 3B) found at the B3LYP-D3/cc-pVDZ-PP with corresponding ECP. Carbon (black), nitrogen (blue), oxygen (red), hydrogen (white), argon (teal), and xenon (purple).

https://doi.org/10.26434/chemrxiv-2023-4vtc9 **ORCID:** https://orcid.org/0000-0001-5960-056X Content not peer-reviewed by ChemRxiv. **License:** CC BY 4.0